Annales
Geophysicae

Intensive radiosonde observations of gravity waves in the lower atmosphere over Yichang (111°18′ E, 30°42′ N), China

Shao Dong Zhang[1,2,3]**, Fan Yi**[1,2,3]**, Chun Ming Huang**[1,2,3]**, and Ze Yu Chen**[4]

[1]School of Electronic Information, Wuhan University, Wuhan, Hubei, People's Republic of China
[2]Key Laboratory of Geospace Environment and Geodesy, Ministry of Education, Wuhan, Hubei, People's Republic of China
[3]State Observatory for Atmospheric Remote Sensing, Wuhan, People's Republic of China
[4]Institute of Atmospheric Sciences, Chinese Academy of Sciences, Beijing, People's Republic of China

Abstract. The characteristics of dynamical and thermal structures and inertial gravity waves (GWs) in the troposphere and lower stratosphere (TLS) over Yichang (111°18′ E, 30°42′ N) were statistically studied by using the data from intensive radiosonde observations in August 2006 (summer month) and January 2007 (winter month) on an eight-times-daily basis. The background atmosphere structures observed in different months exhibit evident seasonal differences, and the zonal wind in winter has a prominent tropospheric jet with a maximum wind speed of about $60\,\mathrm{ms}^{-1}$ occurring at the height of 11.5 km. The statistical results of the inertial GWs in our two-month observations are generally consistent with previous observations in the mid-latitudes. In the summer month, the mean intrinsic frequency and vertical wavelength of the inertial GWs in the troposphere are still larger than those in the lower stratosphere with the absence of intensive tropospheric jets, suggesting that the Doppler shifting due to the tropospheric jets cannot completely account for the differences between the GWs in the troposphere and lower stratosphere. Compared with the observations in the summer month, some interesting seasonal characteristics of the GWs are revealed by the observations in the winter month: 1) more and stronger tropospheric GWs are observed in the winter month; 2) less and weaker GWs are observed in the lower stratosphere in winter; 3) the ratio of the mean GW kinetic energy density to potential energy density is smaller than 1 in winter, which contrasts to that in summer. Most of the seasonal differences can be explained by the intensive tropospheric jets in winter. In both the summer and winter months, the fitted spectral slopes of the vertical wave number spectra for GWs are generally smaller than the canonical spectral slope of −3. Correlation analyses suggest that the tropospheric jet induced wind shear is the dominant source for GWs in both the troposphere and lower stratosphere. Moreover, the tropospheric (lower stratospheric) GWs are found to be modulated by the quasi-7-day (10-day) PW, and the impacts of the diurnal tide on the GWs are relatively weak.

Keywords. Meteorology and atmospheric dynamics (Middle atmosphere dynamics; Waves and tides; General or miscellaneous)

1 Introduction

The lower atmosphere is frequently disturbed by atmospheric waves, including gravity waves (GWs), tidal waves and planetary waves (PWs). These waves are believed to impact significantly local atmospheric climatology (Alexander and Pfister, 1995; Alexander, 1998). Moreover, PWs and GWs have been confirmed to contribute greatly to drive the tropical Quasi-Biennial Oscillation (QBO) and Semi-Annual Oscillation (SAO) (Dunkerton, 1997; Ray et al., 1998).

Now it is widely accepted that GWs in the middle and upper atmosphere (MUA) play an important role in determining the local and global dynamical and thermal structures of the MUA (Lindzen, 1981; Holton, 1982, 1983; Fritts and Vincent, 1987). It has been estimated that on a monthly average GWs provided forcing on the order of $100\,\mathrm{ms}^{-1}\,\mathrm{day}^{-1}$, which is responsible for the wind reversal around the mesopause and the cold summer mesopause (Lindzen, 1981), and they are also partly responsible for driving the Mesospheric Semi-Annual Oscillation (MSAO) (Dunkerton, 1982). It should be noted that GWs propagating in the MUA were believed to be generated mainly in the troposphere and lower stratosphere (TLS) by different

Correspondence to: Shao Dong Zhang
(zsd@whu.edu.cn)

sources, such as convection, tropospheric jet and topography, etc. (Fritts and Alexander, 2003). Recently, many modeling and observational studies have emphasized the importance of the knowledge of the tropospheric GWs in understanding global atmospheric dynamics (Manzini and McFarlane, 1998; Beres et al., 2005; Zhang and Yi, 2005, 2007). Hence, it is of significant importance to study the properties of GWs in the TLS.

Radiosonde observations contribute greatly to our understanding of GWs in the TLS (Tsuda et al., 1994b; Shimizu and Tsuda, 1997; Pfenninger et al., 1999; Vincent and Alexander, 2000; Yoshiki and Sato, 2000; Zink and Vincent, 2001a, b; Innis et al., 2004; Wang et al., 2005; Zhang and Yi, 2005, 2007; Zhang et al., 2006) because of their excellent height resolution (several tens to hundreds of meters) and relatively complete physical quantities. In the above cited observations, the adopted data were mainly from routine measurements made on a twice daily basis by meteorology stations, and the usual method of GW extraction follows closely Allen and Vincent (1995), in which the GW parameters (intrinsic frequency, amplitude, wave vector and energy density) are specified from individual measured profiles of wind and temperature fields by applying dispersion and polarization equations of GWs. The radiosonde data from the routine observation of meteorological agencies usually have a long-term accumulation and broad geographical coverage, which can provide the seasonal and geographical variations of GWs in the TLS. However, it is noteworthy that since the temporal intervals of the twice daily radiosonde routine measurements are usually 12 h, neither the diurnal variations of the dynamical and thermal structures of lower atmosphere nor the short-term (with time scale no longer than 1 wave period) evolutions of GWs can be revealed by these observations. Recently, data from intensive radiosonde observations were used to study the lower atmospheric structures and waves (Tsuda et al., 1994a, b; Seidel et al., 2005), but these observations are generally sparse. In order to further investigate the short-term variation of the lower atmosphere, more radiosonde observations with shorter time interval are needed.

Aiming at further investigation of the lower atmospheric dynamics, especially the lower atmospheric waves and their interactions, a two-month (August 2006 and January 2007) radiosonde observation campaign was launched by Wuhan University. In this campaign, the radiosonde observations were made at Yichang (111°18′ E, 30°42′ N) on an eight-times-daily basis. Compared with the routine radiosonde observation (based on twice daily measurements) made by meteorological agencies, the data from this campaign have a shorter time interval, which permits us to study the propagation and evolution of inertial GWs, tides and PWs.

In the presented paper, we focus primarily on GW activity in the TLS. A detailed introduction of the data set utilized in this paper and the data processing method for extracting wave disturbances are described in the following section. Be-

cause wave excitation and propagation are closely linked to the local dynamical and thermal structures, the background wind and temperature fields are analyzed and presented in Sect. 3. The results of the observed GWs in the summer (August 2006) and winter (January 2007) months are given, respectively, in Sects. 4 and 5. The modulations of GWs by the PWs and tides are discussed in Sect. 6. In the last section, we give a brief summary of our observations.

2 Data description and processing method

The data utilized in this paper are from a two-month (August 2006 and January 2007) radiosonde observation campaign launched by Wuhan University. In this campaign, the radiosonde observations were made at Yichang (111°18′ E, 30°42′ N) on an eight-times-daily basis at 01:00, 04:00, 07:00, 10:00, 13:00, 16:00, 19:00 and 22:00 LT. The raw data are sampled at a 1–2 s interval, resulting in an uneven height resolution, which varies from several to tens of meters. For convenience, in this paper the raw data were processed to have an even height resolution (50 m) by applying a linear interpolation to temperature and pressure data and a cubicspline interpolation to wind measurements. In each measurement by radiosonde, meteorological variables such as pressure, temperature and relative humidity are measured. The horizontal winds can be attained by tracking the position of the balloon, which allows us to determine the horizontal propagation direction of GWs. The adopted data set consists of 241 measurements in August 2006 and 240 measurements in January 2007. The typical height coverage of the radiosonde observation is from the surface up to about 25–40 km, and the uncertainty of the upper height is due to the variable burst height of the balloon. In our data set, more than 70% of the measurements reached a height of 25 km, but only about 50% reached 27 km. Thus, we chose 25 km as the upper height limit of our analysis.

The employed GW extraction and analysis method in this paper is the same as that presented by Zhang and Yi (2005, 2007), which follows closely Allen and Vincent (1995) and Vincent et al. (1997). Here we introduce briefly the extraction method of inertial GWs. Firstly, for obtaining the parameters for quasi-monochromatic GWs, we should correctly remove the background fields $[u_0, v_0, T_0]$ from the raw data, which is calculated by fitting a second-order polynomial to the vertical profiles of horizontal winds and temperature $[u, v, T]$, respectively. To avoid the extreme values of temperatures around the tropopause and those of horizontal winds around the tropospheric jets, the fits are performed for two separate height ranges: a tropospheric segment from 1 to 9 km, and a lower stratospheric segment from 19 to 25 km.

The fluctuation components $[u_f, v_f, T_f]$ are derived from the raw data $[u, v, T]$ by removing the fitted background field. In principle, when we remove the mean wind and

temperature fields from individual profiles, the residuals should consist of a superposition of GWs with different vertical scales; thus, the fluctuation components $[u_f, v_f, T_f]$ are employed to calculate the vertical wave number spectra of the GW fields, which will be discussed in Sects. 4.2 and 5.2. In order to extract quasi-monochromatic GWs, which has a single vertical wavelength, we perform a Lomb-Scargle spectral analysis (Scargle, 1982) on the residuals (e.g. the fluctuation components $[u_f, v_f, T_f]$) to determine the vertical wavelength λ_z. Obviously, the dominant vertical wavelengths derived from different wave components (e.g. zonal wind, meridional wind and temperature) may be different; therefore the average value of these three dominant wavelengths is taken to be the wavelength of the extracted quasi-monochromatic GW. Moreover, only when the relative standard error of these three dominant wavelengths is less than 20% do we consider a quasi-monochromatic GW to be observed. Having specified the vertical wavelength, we take a harmonic fitting to the fluctuation components $[u_f, v_f, T_f]$ to determine the wave amplitudes $[u', v', T']$ and phases for each wave component.

The hodograph of the fitted horizontal wind disturbances is an ellipse. By analyzing the polarization relation for inertial GWs, we know that the ratio of the major to minor axes of the hodograph is equal to the ratio of Ω to f (Tsuda et al., 1990; Eckermann, 1996), where Ω and f denote the wave intrinsic frequency and local Coriolis frequency, respectively. Then the wave intrinsic frequency Ω can be easily calculated from the ellipse. However, a ratio of Ω to f which is too large will cause many uncertainties (Vincent and Alexander, 2000; Zink and Vincent, 2001a), thus, a typical cut off ratio of 10 is chosen in this paper. In addition, anti-clockwise and clockwise rotating hodographs indicate that the GW energy is, respectively, downward and upward propagating in the Northern Hemisphere. Moreover, the horizontal propagation direction of a GW can also be specified from the hodograph, which is along the major axis of the ellipse. The horizontal wave number is deduced from a simplified dispersion equation for inertial GWs, that is

$$k_{zonal}^2 + k_{meridional}^2 = \frac{k_{vertical}^2 (\Omega^2 - f^2)}{N^2}, \tag{1}$$

where k_{zonal}, $k_{meridional}$ and $k_{verical}$ are the zonal, meridional and vertical wave numbers, respectively. The signs of horizontal wave numbers can be derived from the polarization of GWs. N is the buoyance frequency. The signs of the horizontal wave numbers can be derived from the polarization relation of GWs. Zonal, meridional and vertical wave kinetic energy density per unit mass, i.e. E'_{Kzonal}, $E'_{Kmeridional}$ and $E'_{Kvertical}$ are computed from

$$E'_{Kzonal} = \frac{1}{2}u'^2, \tag{2}$$

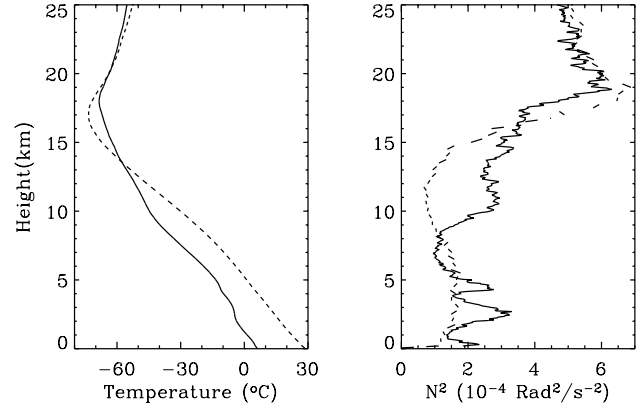$$E'_{Kmeridional} = \frac{1}{2}v'^2 \tag{3}$$

Fig. 1. Monthly averaged temperatures (left panel) and squares of buoyancy frequency (right panel). The dotted and solid curves represent the observation values in summer (August 2006) and winter (January 2007), respectively.

and

$$E'_{Kvertical} = \frac{1}{2}w'^2, \tag{4}$$

respectively. The total wave kinetic energy density per unit mass is $E'_K = E'_{Kzonal} + E'_{Kmeridional} + E'_{Kvertical}$. We have no measurements of vertical wind, but in fact compared with the horizontal wind, it is much smaller and does not contribute significantly to wave energy. Therefore, in our computation of wave kinetic energy, $E'_{Kvertical}$ is omitted. The wave potential energy density per unit mass E'_P is calculated from

$$E'_P = \frac{1}{2}\frac{g^2 T'^2}{N^2 T_0^2}, \tag{5}$$

where g is the gravitational acceleration ($g=9.8\,\text{ms}^{-2}$). The total energy density E' is the sum of E'_K and E'_P.

3 Background observation

Figure 1 shows the monthly averaged temperatures and squares of the buoyancy frequency (N^2) over Yichang in summer (August 2006) and winter (January 2007). It is shown in Fig. 1 that, compared with that in summer, the tropopause (defined as the minimum temperature) in winter is higher and warmer. For the vertical profiles of the N^2, although no obvious seasonal differences in the lower stratosphere (from about 19 to 25 km) are observed, they are rather different in the troposphere in different seasons. For instance, the tropospheric N^2 in summer is almost a constant value about $1.5\times10^{-4}\,\text{rad\,s}^{-1}$; while in winter, the value is much larger and exhibits significant height variation, which may be the result of the frequently occurring tropospheric inversion
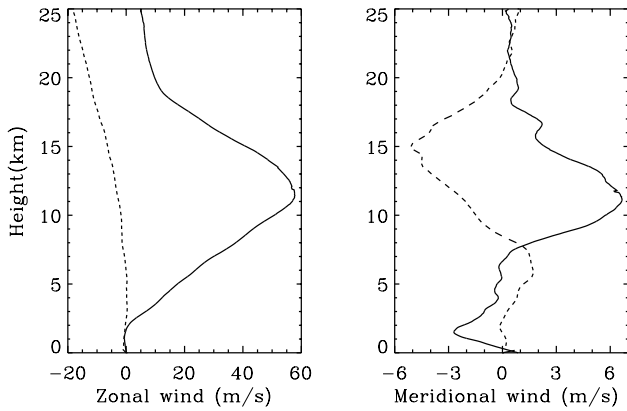
Fig. 2. Monthly averaged zonal (left panel) and meridional winds (right panel). The dotted and solid curves represent the observation values in summer (August 2006) and winter (January 2007), respectively.
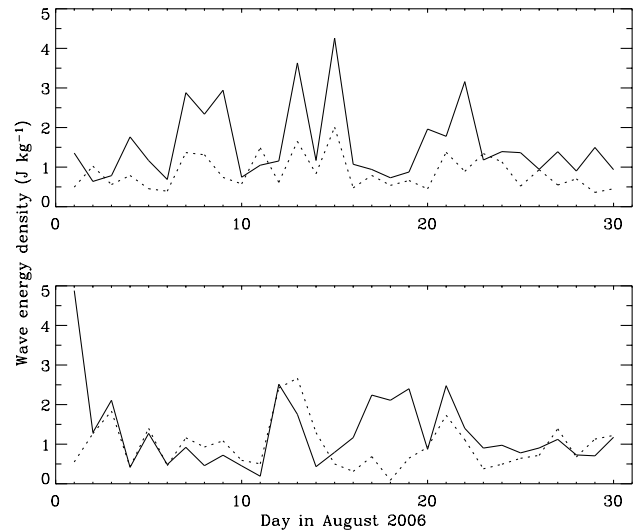

Fig. 3. Daily averaged GW kinetic energy (solid curves) and potential energy (dotted curves) densities in the troposphere (bottom panel) and lower stratosphere (top panel) in August 2006.

layers in winter (a detailed analysis about the winter tropospheric inversion layers was given by Zhang et al. (2008)[1].

The monthly averaged horizontal wind profiles over Yichang in winter and summer are plotted in Fig. 2. In summer the averaged zonal wind is westward, and its magnitude increases with height and is no larger than $20\,\mathrm{ms^{-1}}$. While in winter, much larger eastward zonal wind can be observed, and a prominent tropospheric jet with a maximum wind speed of about $60\,\mathrm{ms^{-1}}$ occurs at the height of $11.5\,\mathrm{km}$. Compared with the zonal winds, the meridional winds are quite weaker. Moreover, the summer and winter meridional wind directions are opposite in almost all the height coverage.

4   Inertial GWs in the summer month

4.1   Wave parameters

By employing the analysis method introduced in Sect. 2, more than $140\,\mathrm{GW}$ events in the troposphere and lower stratosphere were extracted from 241 measurements in the summer month, and their statistical parameters are listed in Table 1, which are generally consistent with the observations in the mid-latitudes (Wang et al., 2005; Zhang and Yi, 2005, 2007). As shown in Table 1, the fraction of upward propagation in the troposphere is 41.1%, smaller than the values (about 50%) reported by Zhang and Yi (2005, 2007), in which the mean GW parameters were estimated from an average over several years of observations. Sources located in the heights above the tropospheric segment may be respon-

sible for the smaller upward propagation fraction of GWs in the troposphere. Moreover, one can observe from Table 1 that the number of observed GW events and the fraction of upward propagation in the troposphere (141 and 41.1%, respectively) are, respectively, smaller than those in the lower stratosphere (176 and 86.9%, respectively), implying that there are additional sources for GWs in the lower stratosphere in the intermediate region between the tropospheric and lower stratospheric segments (e.g. from 9 to 19 km).

Another interesting result shown in Table 1 is that the mean intrinsic frequency and vertical wavelength in the troposphere are smaller than those in the lower stratosphere. Such a difference has been revealed by several previous observations (Wang et al., 2005; Zhang and Yi, 2005, 2007) and was attributed to the Doppler shifting of the tropospheric jet (Vincent and Alexander, 2000; Wang et al., 2005). However, it should be emphasized that in our summer observations, the horizontal wind and its vertical shear are rather small, indicating the Doppler shifting of the background wind doesn't contribute greatly to this difference. Comprehensive understanding of the differences between the GWs in the troposphere and lower stratosphere needs a combination of considerations of the vertical structures of background atmosphere (wind and temperature fields) and the GW source features.

Moreover, we want to note that in our previous observations (Zhang and Yi, 2005, 2007), the averaged ratios of E'_K to E'_P in the troposphere are smaller than 1, and it is difficult to explain this from the GW theory, which predicts that for a steadily and freely propagating GW, the ratio of E'_K to E'_P should be slightly larger than 1. This discrepancy has been presumed to result from the fact that in the mid-latitudinal region, the tropospheric jet is one of the primary source of

---

[1]Zhang, Y. H., Zhang, S. D., and Yi, F.: Intensive radiosonde observations of lower tropospheric inversion layers over Yichang (111°18′ E, 30°42′ N), China, J. Atmos. Sol.-Terr. Phys., in review, 2008.

Table 1. Mean values of GW parameters in August 2006. λ_z, λ_x and λ_y stand for the vertical, zonal and meridional wavelengths, respectively; the over bars denote an unweighted average.

	Tropospheric segment	Lower stratospheric segment
GW events	141	176
Fraction of upward propagation (%)	41.1	86.9
$\overline{\dfrac{\Omega}{f}}$	3.9	3.2
$\overline{u'}$ (ms^{-1})	1.3	1.4
$\overline{v'}$ (ms^{-1})	1.4	1.6
$\overline{T'}$ (K)	0.6	0.8
$\overline{\lambda_z}$ (km)	4.2	3.1
$\overline{\lambda_x}$ (km)	458	725
$\overline{\lambda_y}$ (km)	504	787
$\overline{E'}$ (J kg^{-1})	2.2	2.3
$\overline{E'_K \big/ E'_P}$	1.1	1.8

inertial GWs in the lower atmosphere, hence the tropospheric GWs are probably within or in the vicinity of the source region (freshly generated) and far from the status of free propagation (Zhang and Yi, 2007), whereas in the present summer observations, this ratio is larger than 1, implying that in summer, there may be other dominant sources for the tropospheric GWs located in a relatively further region from the tropospheric segment, for instance, in the intermediate segment or the stratosphere.

The daily averaged wave energy densities and the monthly averaged local time variations of the wave energy densities are plotted in Figs. 3 and 4, respectively. Figure 3 illustrates that the kinetic wave energy are generally larger than the potential energy in both the troposphere and lower stratosphere, and both the kinetic and potential energy densities exhibit quite irregular day-to-day variations, which reflect the complexity of the wave sources in summer. Certainly, besides the source variation, the variation of the background flow and thermal structure and even the planetary wave modulation may induce the day-to-day variation of GW energy. The results shown in Fig. 4 reveal that the GW energies also exhibit evident local time variation. For waves in the troposphere, the kinetic energy density has an almost opposite local time variation to that of the potential energy density, and its three peak values occur at 07:00, 11:00 and 19:00 LT, respectively. As to the waves in the stratosphere, the kinetic energy density exhibits an evident diurnal variation, and its maximum (1.9 kg^{-1}) and minimum (1.0 J kg^{-1}) values occur at 04:00 and 13:00 LT, respectively, which is presumably due to the joint actions of the diurnal variation of the source and background atmosphere and the modulation of the diurnal tide. However, the confirmation of this speculation needs more quantitative analyses, which will be presented in Sect. 6.
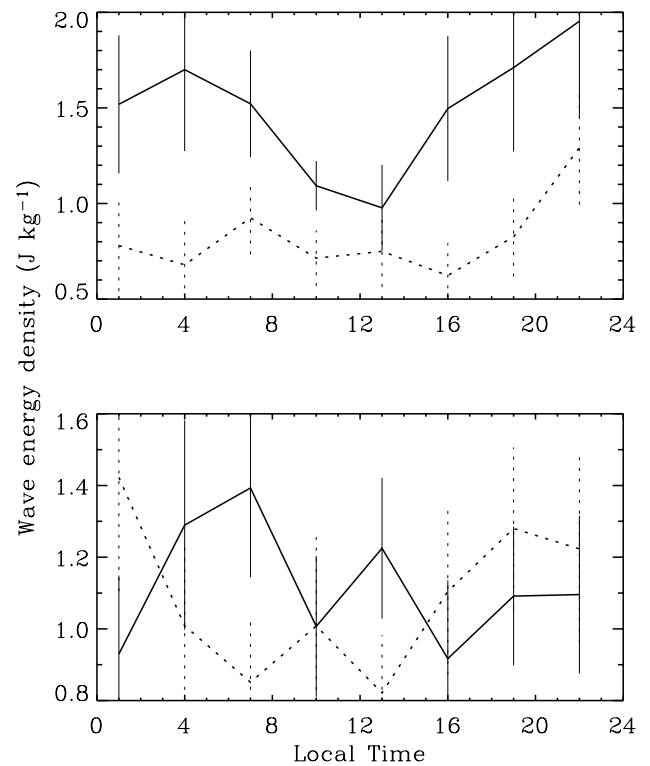

Fig. 4. Monthly averaged local time variations of the GW kinetic energy (solid curves) and potential energy (dotted curves) densities in the troposphere (bottom panel) and lower stratosphere (top panel) in August 2006. The vertical lines denote the standard deviation.

4.2 Vertical wave number spectra

In order to investigate the spectral characteristics of the inertial GWs, we perform a Fourier transform on zonal wind
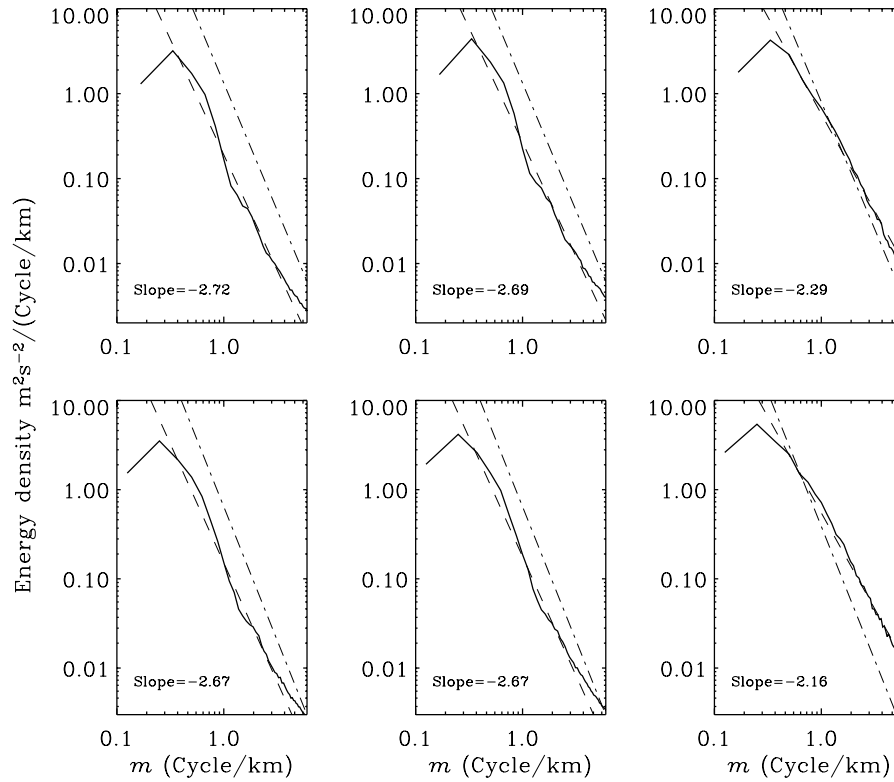
Fig. 5. Averaged vertical wave number spectra (solid curves) for the zonal kinetic energy density (left column), meridional kinetic energy density (middle column) and potential energy density (right column) in the troposphere (bottom row) and lower stratosphere (top row) in August 2006. The dashed lines denote the fitted spectra. The theoretical saturation limits of Smith et al. (1987) are also plotted for comparison purposes (dash-dotted lines).

Table 2. Parameters of vertical wavenumber spectra for GWs in the troposphere and lower stratosphere over Yichang station in August 2006. q represents the slope of the vertical wavenumber spectrum in the large wavenumber regions. m_* (in (Cycle/km)) and E_* (in $m^2\, s^2$/(Cycle/km)) denote the characteristic vertical wavenumber and the corresponding spectral intensity.

| | u_f | | | v_f | | | $\frac{gT_f}{\overline{N}T_0}$ | | |
	q	m_*	E_*	q	m_*	E_*	q	m_*	E_*
Troposphere	−2.67	0.25	3.52	−2.67	0.25	4.17	−2.16	0.25	5.41
Lower stratosphere	−2.72	0.33	3.20	−2.69	0.33	4.42	−2.29	0.33	4.26

(u_f), meridional wind (v_f) and weighted temperature ($\frac{gT_f}{\overline{N}T_0}$) fluctuations, where $\overline{N}$ is the unweighted height and temporal average of the buoyancy frequency N. In the estimates of the power spectral amplitudes, for the purpose of improving the confidence limits, the vertical wave number power spectra calculated from individual profiles are averaged, while in the calculation of the mean spectrum, in order to ensure that all spectra contribute equally to the shape of the mean spectrum, normalized individual power spectra are averaged as the mean spectrum (Allen and Vincent, 1995). Figure 5 illustrates the averaged vertical wave number spectra for the

zonal wind (left column), meridional wind (middle column) and weighted temperature (right column) in the troposphere (bottom row) and lower stratosphere (top row) over Yichang station in August 2006, and the spectral parameters are listed in Table 2. As a comparison, the theoretical saturation spectra (Smith et al., 1987) are also plotted in Fig. 5. According to the saturation spectrum theory (Smith et al., 1987; Allen and Vincent, 1995; Fritts and Alexander, 2003, and references herein), in the saturation region ($m > m_*$, where m is the vertical wave number; and m_* is the characteristic vertical wave number, which is the vertical wave number of the most energetic GW), the theoretical vertical wave number spectrum of

GW kinetic and potential energies, i.e. $E_K(m)$ and $E_P(m)$, can be respectively expressed as

$$E_K(m) \approx \frac{pN^2}{10\,m^3} \qquad (6)$$

and

$$E_P(m) \approx \frac{N^2}{6\,pm^3}, \qquad (7)$$

where p is the slope of the one-dimension frequency spectrum. The best estimate of p from previous literature is $5/3$, and this value will be assumed hereinafter. In the calculation of the theoretical spectra, the buoyancy frequencies N are replaced by the values of $\overline{N}$.

Figure 5 illustrates that each spectrum density has two distinct regions, which are partitioned by spectral knees (characteristic wave number m_*). In both the troposphere and lower stratosphere, the characteristic wave numbers for different wave components (zonal wind, meridional wind and temperature) have consistent values, which are 0.25 and 0.33 Cycle/km (listed in Table 2), respectively, corresponding to the dominant vertical wavelengths of 4.0 and 3.0 km, respectively. The dominant vertical scales estimated from the spectra are close to the mean vertical wavelengths shown in Table 1, which are 4.2 and 3.1 km, respectively. And Fig. 5 also exhibits considerable conformity between the spectra in the troposphere and the lower stratosphere. Firstly, the spectral intensities in the troposphere and lower stratosphere are close to each other and are much smaller than the averaged values over several years worth of routine radiosonde observations (Zhang et al., 2006), which might be attributed to the weak GW activity in summer. In the troposphere, the maximum spectral amplitudes E_* (the spectral intensity corresponding to the characteristic wave number) for the zonal, meridional kinetic and potential energy densities are about 3.42, 4.17 and 5.41 m^2 s^{-2}/(Cycle/km), respectively. In the lower stratosphere, the corresponding values are 3.20, 4.42 and 4.26 m^2 s^{-2}/(Cycle/km), respectively. Secondly, at the small m region ($m < m_*$), spectral densities increase with wave number. For the large m region ($m > m_*$), spectral densities decrease with wave number, and the fitted slopes for each spectrum vary from -2.16 to -2.72, which are smaller in magnitude (hereinafter, when we discuss the slope, we refer to its magnitude) than the canonical spectral slope of -3 (Dewan et al., 1984; Dewan and Good, 1986; Smith et al., 1987). Additionally, compared with those of the kinetic energy, the spectra of the potential energy density exhibit larger spectral magnitudes and shallower slopes. The conformity between the spectra in the troposphere and the lower stratosphere can be explained by the fact that the zonal background wind in summer is rather weak and has only a slight impact on GWs. Furthermore, compared with the theoretical saturation spectra, the observed spectra in summer have smaller spectral magnitudes. Such a discrepancy might be due to the fact that the lower atmospheric GW activity in summer is

rather weak, and their amplitudes are much smaller than the saturation threshold.

4.3 Wave sources

The correlation coefficient between the time series of the daily averaged wave energy densities for GWs in the troposphere and lower stratosphere is a small value of 0.12. Aiming at investigating the possible generation sources of GWs in the TLS, we calculate, respectively, the vertical profiles of the correlation coefficients between the GW energy densities and the vertical shear of horizontal wind ($s = \left(\frac{\partial u_0}{\partial z}\right)^2 + \left(\frac{\partial v_0}{\partial z}\right)^2$) and the square of the buoyancy frequency for the moist air (N_m^2). The correlation analyses are processed as follows: firstly, we calculate the time series of daily averaged GW energy densities in the troposphere and lower stratosphere, respectively; secondly, we calculate, respectively, the time series of daily averaged s and N_m^2 at each sampling heights; finally, at each sampling heights, we calculate the correlation coefficients between the GW energy density and the wind shear and the square of the buoyancy frequency for the moist air, respectively. Therefore, we can obtain the correlation coefficients in the whole height range of 0–25 km. Moreover, we want to note here that the adoption of the buoyancy frequency for the moist air instead of the dry air is to investigate the contribution of convection in GW generation. The results are plotted in Fig. 6. In the calculation of the correlation coefficients, the daily averaged values of the wave energy densities, vertical shear of the horizontal wind, and square of the buoyancy frequency for the moist air are used.

One can observe from Fig. 6 that for GW activity in the troposphere, the possible dominant source, is the vertical shear of the horizontal wind in the tropospheric segment, while for GWs, in the lower stratosphere, large correlation between the wave density and the vertical shear of the horizontal wind is observed in the height range from 18 to 23 km. Additionally, the correlation coefficients between the N_m^2 and GW densities are larger than 0.5 at several heights in the troposphere, suggesting convection may contribute to the excitation of GWs in the summer month.

5 Inertial GWs in the winter month

5.1 Wave parameters

For GW activity in the winter month (January in 2007), their statistical parameters are summarized in Table 3. It is found from Table 3 that the number of observed GW events in the troposphere is 178, which is larger than that in summer (as shown in Table 1). This is due to the greater excitations of GWs by the intensive tropospheric jet in winter. However, resulting from the jet-induced filtering effect, the lower stratospheric GWs is less than that in summer, indicating the

Table 3. Similar to Table 1, but for waves in January 2007.

	Tropospheric segment	Lower stratospheric segment
GW events	178	164
Fraction of upward propagation (%)	44.4	77.4
$\overline{\dfrac{\Omega}{f}}$	3.7	3.1
$\overline{u'}$ (ms^{-1})	3.0	1.4
$\overline{v'}$ (ms^{-1})	2.6	1.3
$\overline{T'}$ (K)	1.4	1.1
$\overline{\lambda_z}$ (km)	4.2	3.2
$\overline{\lambda_x}$ (km)	580	711
$\overline{\lambda_y}$ (km)	468	672
$\overline{E'}$ (J kg^{-1})	12.3	2.5
$\overline{E'_K}\big/\overline{E'_P}$	0.72	0.74
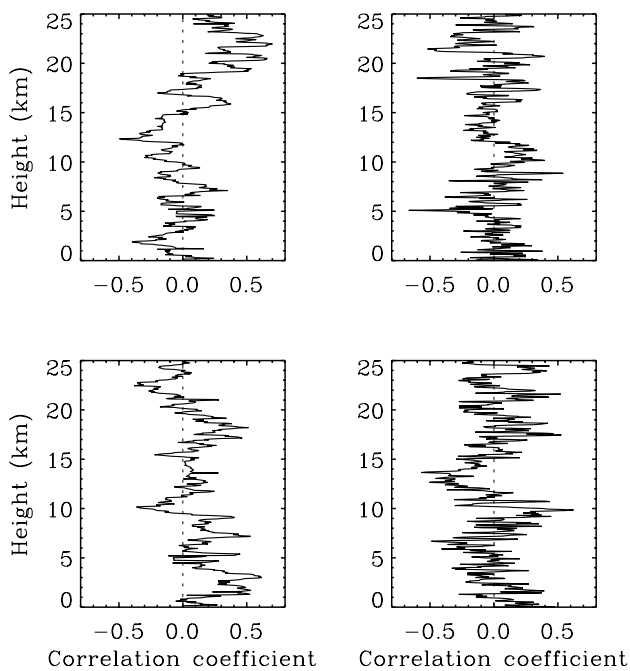
Fig. 6. Profiles of correlation coefficients of vertical shear of the horizontal wind (left column) and square of the buoyancy frequency of the moist air (right column) with GW energy densities in the troposphere (bottom row) and lower stratosphere (top row) in August 2006.

important role of the tropospheric jet in the excitation and propagation of the lower atmospheric inertial GWs.

Compared with the mean vertical wavelengths in summer (as listed in Table 1), almost the same values can be observed in winter, indicating that there are no obvious seasonal variations of the vertical wavelength. These results are consistent with previous radiosonde observations (Zhang and Yi, 2007;

Wang et al., 2005), and their exact cause is unclear at the current stage. However, these results, at least, reveal that the Doppler shifting can only provide a qualitative explanation of the variations for the character of the lower atmospheric GWs. Similarly, seasonal consistence can also be found in the average intrinsic frequency and horizontal wavelengths.

The most striking result shown in Table 3 is the wave energy density. Firstly, although the averaged lower stratospheric wave energy density in winter is very close to that in summer, unusually large GW energy is observed in the winter troposphere, which is due to the more intensive source (for instance, the tropospheric jet) in winter. Moreover, Table 3 reveals that the ratio of the averaged E'_K to E'_P is smaller than 1, which is completely opposite to the result in summer. As suggested by Zhang and Yi (2005, 2007), the small ratios of E'_K to E'_P indicate that in winter, GWs in the TLS are probably within or in the vicinity of the source region (or freshly generated) and far from the status of free propagation.

The daily averaged and monthly averaged local time variations of wave energy densities are plotted in Figs. 7 and 8, respectively. Figure 7 reveals that wave energy density in the lower stratosphere is evidently smaller than that in the troposphere, which results from the background absorption of wave energy due to the strong tropospheric jet in winter. For wave energy in the troposphere, the potential energy density is evidently larger than the kinetic energy density, and its two prominent peaks occur on 6 January and 24 January, respectively, corresponding to the durations of two lower tropospheric inversion events. The close relation between the strong GW activity and the lower tropospheric inversion events was discussed in detail by Zhang et al. (2008)[1]. These two peak values are about 30 J kg^{-1}, which are one order larger than the yearly averaged value at Yichang (Zhang and Yi, 2007). Such a large potential energy density has been seldom reported. Similar local time variations of the energy

Table 4. Similar to Table 2, but for GWs in January 2007.

	u_f			v_f			$\frac{gT_f}{NT_0}$		
	q	m_*	E_*	q	m_*	E_*	q	m_*	E_*
Troposphere	−2.74	0.25	15.32	−2.75	0.25	20.73	−2.35	0.25	42.56
Lower stratosphere	−2.42	0.33	2.53	−2.51	0.33	2.33	−2.29	0.33	6.02
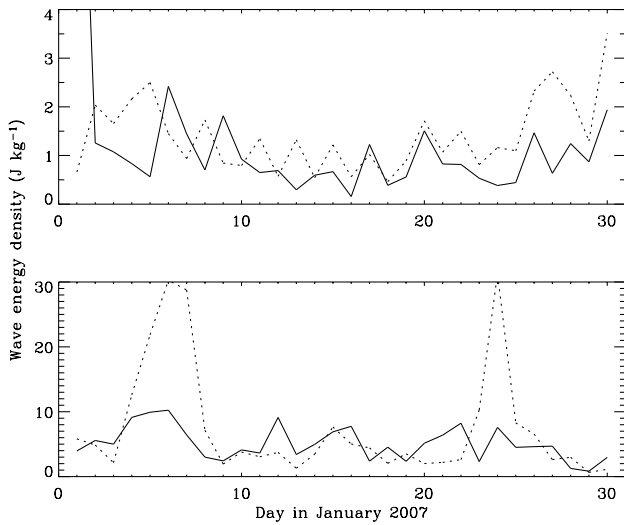
Fig. 7. Similar to Fig. 3, but for GWs in January 2007.

densities for GWs in the troposphere and lower stratosphere are illustrated in Fig. 8, and in both the troposphere and lower stratosphere, the potential energy densities have rather similar local time variation to those of the kinetic energy densities. These similarities suggest the same dominate source for the inertial GWs in the troposphere and lower stratosphere in winter, which have been suggested to be the tropospheric jet (Zhang and Yi, 2005, 2007).

5.2 Vertical wave number spectra

By employing the same method as that introduced in Sect. 4.2, we calculate the vertical wave number spectra of the GWs in January 2007. The spectra and their primary parameters are respectively given in Fig. 9 and Table 4. In the troposphere, consistent characteristic wave number of 0.25 Cycle/km for different wave components (zonal wind, meridional wind and temperature) can be observed, corresponding to a dominant vertical wavelength of 4.0 km. In the lower stratosphere, larger characteristic wave numbers (0.33 Cycle/km) are calculated. Considerably large spectral amplitudes in the troposphere are illustrated in Fig. 9, and in the high wave number region ($m > m_*$), the spectral intensities are rather close to or even larger than those pre-
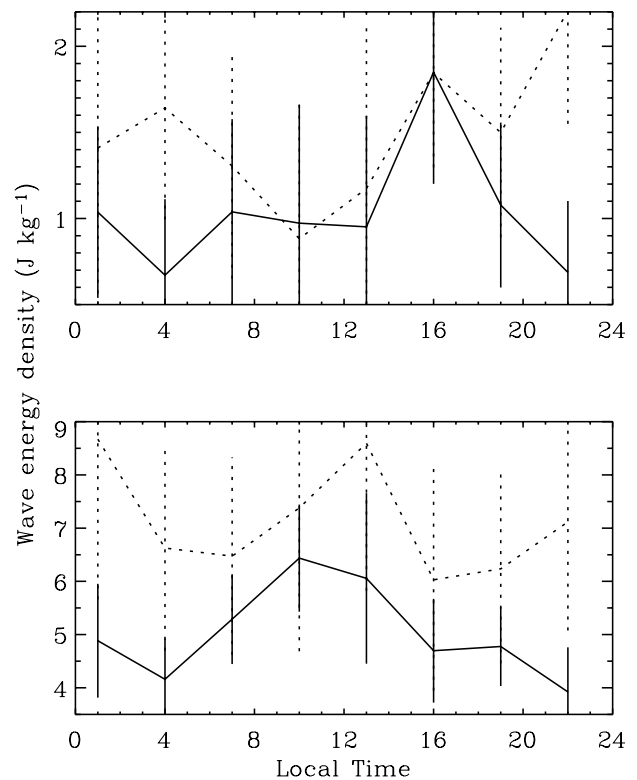

Fig. 8. Similar to Fig. 4, but for GWs in January 2007.

dicted by the saturation spectral theory (Smith et al., 1987). The maximum spectral intensities E_* for the zonal wind, meridional wind and weighted temperature are, respectively, 15.32, 20.73 and 42.56 $m^2\,s^{-2}/(Cycle/km)$, which are evidently larger than those in summer. Although spectral intensities in the troposphere are quite large, the spectral intensities for kinetic energy in the lower stratosphere are rather small, which results from the wave energy absorption of the tropospheric jet. In the large m region ($m > m_*$), the fitted slopes for each spectrum vary from −2.29 to −2.75, which are close to those in the summer month and generally smaller than the canonical spectral slope. Moreover, the slopes of GW in the stratosphere are generally smaller than those in the troposphere, which demonstrates that the strong background wind shear tends to yield shallower slopes (Zhang et al., 2006). Two causes may be responsible for the discrepancy
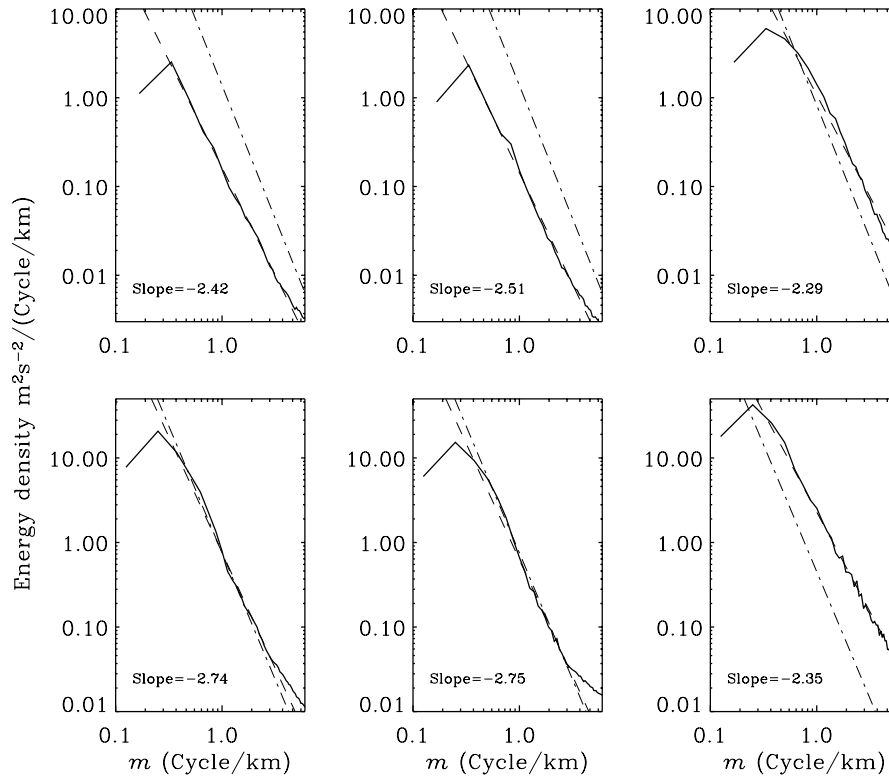
Fig. 9. Similar to Fig. 5, but for GWs in January 2007.

between the slopes from our observations and the canonical spectral slope: 1) the existing spectral theories may not accurately predict the realistic GW field spectral features, especially for inertial GWs. In fact, the departures of the slope from the canonical value of -3 have been revealed by previous observations (e.g. Wilson et al., 1990; Tsuda et al., 1991, 1994b; Senft et al., 1993; Nastrom et al., 1997; de la Torre et al., 1999; Zhang et al., 2006), and these departures seem to be persistent and climatological rather than transitory (e.g. Tsuda et al., 1991; Nastrom et al., 1997; de la Torre et al., 1999; Zhang et al., 2006). 2) The observed GW spectra may be contaminated by nonmigrating tides (Huang et al., 2008[2]), which are usually high order harmonics and have small vertical wavelengths.

Moreover, the spectral amplitudes and dominant wavelengths attained from the presented radiosonde observations are generally in agreement with those from previous radiosonde and MU radar observations (Fritts et al., 1988; Tsuda et al., 1989, 1991) over Shigaraki, Japan (136°06′ E, 35°51′ N), where is in the similar latitudes to that of Yichang (111°18′ E, 30°42′ N). Over both observation sites, the spectral amplitudes in the troposphere and winter are larger than

those in the lower stratosphere and summer, respectively, and the dominant vertical wavelengths in the troposphere are larger than those in the lower stratosphere. As to the spectral slopes, the values over Yichang are slightly smaller than those over Shigaraki.

5.3 Wave sources

In January 2007, the correlation coefficient between the daily averaged GW energy densities in the troposphere and lower stratosphere is 0.56, larger than that in the summer month, indicating that GWs in the troposphere and lower stratosphere may have the same dominant excitation source. The correlation coefficients shown in Fig. 10 also reveal the important role of wind shear in the excitation of GWs. The correlation coefficients between the wind shear and the GW energy densities in both the troposphere and lower stratosphere have prominent large values (larger than 0.7 and 0.9 in the troposphere and lower stratosphere, respectively) below and above the tropospheric jet, suggesting that in winter, the tropospheric jet induced strong shear is the dominant source for GWs in the lower atmosphere. Another interesting result shown in Fig. 10 is that although the GW activity in the lower stratosphere doesn't exhibit evident correlation with the convection, the N_m^2 at 13 km shows a clear negative correlation with the GW activity in the troposphere, indicating that the

---

[2]Huang, C. M., Zhang, S. D., and Yi, F.: Intensive radiosonde observations of the diurnal tide and planetary waves in the lower atmosphere over Yichang (111°18′ E, 30°42′ N), China, Ann. Geophys., submitted, 2008.

convection also plays a role in the excitation of the tropospheric GWs in winter. Moreover, in the height range of 3–5 km, the tropospheric GWs correlate positively with the N_m^2, implying that there is a close correlation between the tropospheric GWs and the lower tropospheric inversion layers, which was discussed in detail by Zhang et al. (2008)[1].

Finally, we want to note that in both months (August 2006 and January 2007), and in both the troposphere and the lower stratosphere, the correlation coefficients between the GW energy densities and the surface flows are very small, no larger than 0.3, indicating that the topography is not the dominant source of GWs in the observation site.

6 Diurnal tide/GW and PW/GW interactions

A great deal of literature (Fritts and Vincent, 1987; Manson et al., 2003; Espy et al., 2004; Innis et al., 2004; Williams et al., 2006) has suggested that there were extensive interactions among atmospheric waves (e.g. GWs, PWs and tidal waves, etc.). By using the data from three radisonde stations at the polar region, Innis et al. (2004) have revealed that GWs in the TLS were modulated by PW, and by using the same data set as adopted in this paper, Huang et al. (2008)[2] analyzed the diurnal tides and PWs and their coupling in the lower atmosphere. The results presented by Huang et al. (2008)[2] indicated that there existed dominant migrating and nonmigrating diurnal oscillations in the TLS over Yichang. Moreover, Huang et al. (2008)[2] also found significant quasi-7-day PW (QSDPW) and quasi-10-day PW (QTDPW) oscillations in both the zonal and meridional winds, in both months, and the maximum amplitudes of these PWs can be larger than $10 \, \text{ms}^{-1}$, which is a significant level. Here, in order to give some insights into the interactions between GWs and other atmospheric waves (diurnal tide and PWs), we calculate the frequency spectra for the time series of the GW energy densities and plot the results in Fig. 11. Since oscillations with periods greater than 20 days are conventionally not classified as PWs because their periods do not conform to those expected for common Rossby modes (Beard et al., 2001), here only the oscillations with periods of 0.5–20 days are presented in Fig. 11, which illustrates several prominent planetary-scale spectral peaks, indicating the intensive coupling between the GWs and PWs. In the summer month, the tropospheric and lower stratospheric GW energy densities exhibit prominent spectral peaks with periods of 9.2 and 6.7 days, respectively. These spectral peaks have been respectively recognized as the quasi-10-day planetary wave (QTDPW) and quasi-7-day planetary wave (QSDPW) by Huang et al. (2008)[2]. Besides the quasi-10-day oscillation, the tropospheric GW energy density in August 2006 has two other obvious spectral components with periods of 5.0 and 3.6 days. For GWs in the winter month, their energy densities show dominant spectral peaks at periods of 8.5 and 5.7 days in the troposphere and lower stratosphere,
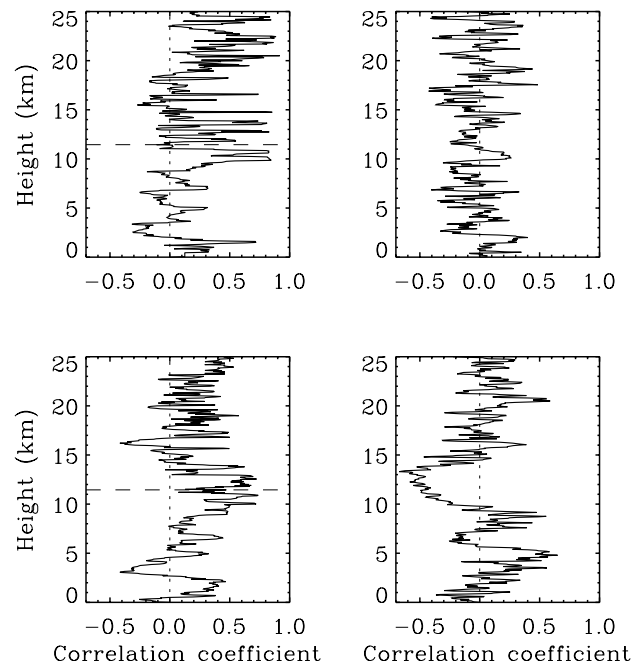

Fig. 10. Similar to Fig. 6, but for correlation coefficients in January 2007. The horzional dashed lines denote the maximum zonal wind height.

respectively. Therefore, as a summary, the lower atmospheric GWs are intensively modulated by PWs, and generally, the tropospheric (lower stratospheric) GWs are modulated primarily by the quasi-7-day (10-day) PW.

As mentioned in Sect. 4.1, several effects, i.e. the wave sources, background flow and thermal structure and planetary wave modulation could produce the day-to-day variations of the GW energy. Essentially, it is difficult to clearly determine which effect is the dominant mechanism from our data set. However, we take into consideration that the effects of the sources and background flow and thermal structure are direct, while the planetary wave modulation may be indirect. And more importantly, the planetary wave itself should be significantly affected by the sources and background flow. Thus, we speculate that the variations of sources and background flow and thermal structure might be the dominant mechanisms responsible for the day-to-day variation of GW energy.

As shown in Fig. 11, the GWs energy densities in our observations also have obvious diurnal spectral components, indicating the GWs are probably modulated by the diurnal tide too. However, the significance levels for the diurnal spectral peaks are generally low, indicating the relatively weak impacts of the diurnal tides on the lower atmospheric GWs.
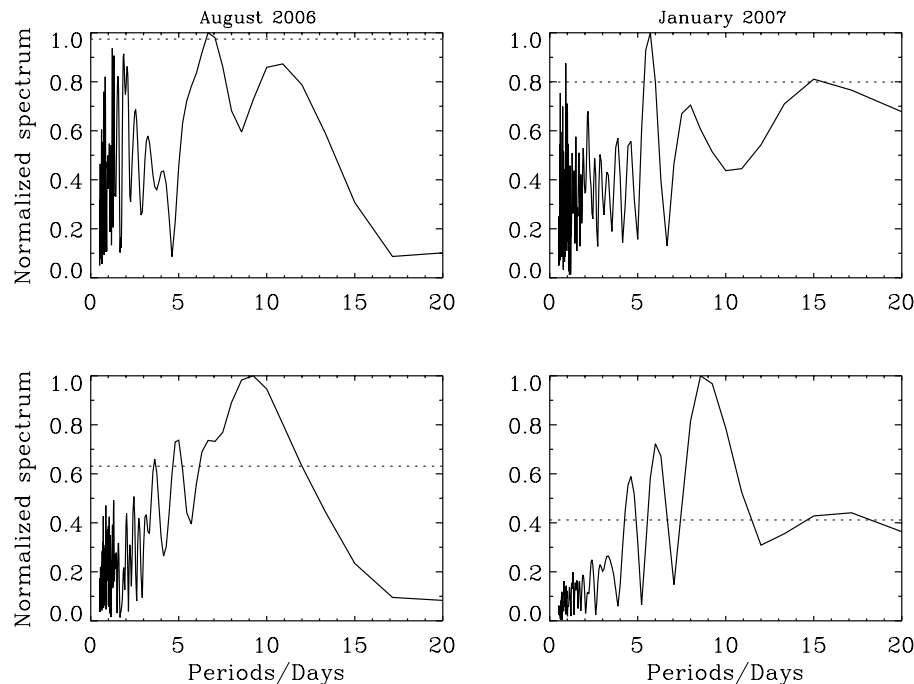
Fig. 11. Normalized frequency spectra of the time series of the tropospheric (bottom row) and lower stratospheric (top row) GW energy densities in August 2006 (left column) and January 2007 (right column). The horizontal dotted lines denote the 90% significance level.

7 Summary

In August 2006 and January 2007, aiming at investigating the lower atmospheric dynamics, we launched an intensive radiosonde observation campaign at Yichang ($111°18'$ E, $30°42'$ N), China. In this campaign, the radiosonde observations were made on an eight-times-daily basis at 01:00, 04:00, 07:00, 10:00, 13:00, 16:00, 19:00 and 22:00 LT. By using the data from this campaign, in this paper we studied the primary features of the dynamical and thermal structures of the background atmosphere and GWs in the TLS over Yichang. The main results of this paper are summarized as follows.

The background atmospheric structures observed in the different months exhibit evident seasonal differences. Compared with that in the summer month (August 2006), the tropopause in the winter month is higher and warmer, and the square of buoyancy frequency in the troposphere in winter is larger and exhibits significant height variation, which may result from the frequently occurring tropospheric inversion layers in winter. In summer, the averaged zonal wind is westward, while a much larger eastward zonal wind is observed in winter. The observed zonal wind in winter has a prominent tropospheric jet with a maximum wind speed of about $60\,\mathrm{ms}^{-1}$ occurring at the height of 11.5 km. In both months, the meridional winds are quite weaker than the zonal winds.

The statistical results of the inertial GWs in our two-month (August 2006 and January 2007) campaign are generally consistent with previous observations in the mid-latitudes (Wang et al., 2005; Zhang and Yi, 2005, 2007), and some interesting seasonal characteristics of the GWs in the TLS are revealed by our observations.

In the summer month, both the number of observed GW events and the fraction of upward propagation in the troposphere are all smaller than those in the lower stratosphere, indicating that there are sources for the lower stratospheric GWs in the intermediate region between the tropospheric and lower stratospheric segments (e.g. from 9 to 19 km). Moreover, the averaged ratio of E'_K to E'_P in the troposphere is larger than 1, implying that there may exist sources for the tropospheric GWs in a relatively further region from the tropospheric segment. Although there are no intensive tropospheric jets in summer, the mean intrinsic frequency and vertical wavelength in the troposphere are still smaller than those in the lower stratosphere, suggesting the Doppler shifting due to the tropospheric jets cannot completely account for the differences between the GWs in the troposphere and lower stratosphere.

In the winter month, although almost the same mean vertical and horizontal wavelengths and intrinsic frequencies as those in the summer month are observed, there are several obvious seasonal differences which should be emphasized: 1) more and stronger tropospheric GWs are observed in the winter month; 2) less and weaker GWs are observed in the

lower stratosphere; 3) the ratio of the average E'_K to E'_P is smaller than 1. Most of the seasonal differences can be explained by the intensive tropospheric jets in winter. The jet in winter can excite more and stronger GWs in the troposphere, but some of the tropospheric GWs are absorbed by the jet.

In both the summer and winter months, the vertical wave number spectra for GWs energy exhibit some departures from the predictions of the saturation spectral theory. The fitted spectral slopes are generally smaller than the canonical spectral slope of -3. Two causes may be responsible for the discrepancy between the slopes from our observations and the canonical spectral slope: 1) the existing spectral theories may not accurately predict the realistic GW field spectral features, especially for inertial GWs; 2) the observed GW spectra may be contaminated by nonmigrating tides.

Correlation analyses suggest that in winter, the troposheric jet induced strong shear is the dominant sources for GWs in both the troposphere and lower stratosephre. Moreover, the convection also plays a role in the excitation of tropospheric GWs. Interestingly, the close correlation between the tropospheric GWs and the lower tropospheric inversion layers is also observed, which is discussed in detail by Zhang et al. (2008)[1].

The GW energies are found to be modulated by the PWs and diurnal tide. Generally, the tropospheric (lower stratospheric) GWs are modulated primarily by the quasi-7-day (10-day) PW, and compared with the PWs, the impacts of the diurnal tide on the GWs are relatively weak.

References

Alexander, M. J.: Interpretations of observed climatological patterns stratospheric gravity wave variance, J. Geophys. Res., 103, 8627–8640, 1998.

Alexander, M. J. and Pfister, L.: Gravity wave momentum flux in the lower stratosphere over convection, Geophys. Res. Lett., 22, 2029–2032, 1995.

Allen, S. J. and Vincent, R. A.: Gravity-wave activity in the lower atmosphere: Seasonal and latitudinal variations, J. Geophys. Res., 100, 1327–1350, 1995.

Beard, A. G., Williams, P. J. S., Mitchell, N. J., and Muller, H. G.: A spectral climatology of planetary waves and tidal variability, J. Atmos. Solar-Terr. Phys., 63, 801–811, 2001.

Beres, J. H., Garcia, R. R., Boville, B. A., and Sassi, F.: Implementation of a gravity wave source spectrum parameterization

dependent on the properties of convection in the Whole Atmosphere Community Climate Model (WACCM), J. Geophys. Res., 110, D10108, doi:10.1029/2004JD005504, 2005.

de la Torre, A., Alexander, P., and Giraldez, A.: The kinetic to potential energy ratio and spectral separability from high resolution balloon soundings near the Andes mountains, Geophys. Res. Lett., 26, 1413–1416, 1999.

Dewan, E. M. and Good, R. E.: Saturation and the "universal" spectrum for vertical profiles of horizontal scalar winds in the atmosphere, J. Geophys. Res., 91, 2742–2748, 1986.

Dewan, E. M., Grossbard, N., Quesada, A. F., and Good, R. E.: Spectral analysis of 10 m resolution scalar velocity profiles in the stratosphere, Geophys. Res. Lett., 11, 80–83, 1984.

Dunkerton, T. J.: Theory of the mesopause semiannual oscillation, J. Atmos. Sci., 39, 2681–2690, 1982.

Dunkerton, T. J.: The role of gravity waves in the quasi-biennial oscillation, J. Geophys. Res., 102(D22), 26 053–26 076, 1997.

Eckermann, S. D.: Hodograph analysis of gravity waves: Relationships among Stokes parameters, rotary spectra and cross-spectral methods, J. Geophys, Res., 101, 19 169–19 174, 1996.

Espy, P. J. and Jones, G. O. L.: Tidal modulation of the gravity-wave momentum flux in the Antarctic mesosphere, Geophys. Res. Lett., 31, L11111, doi:10.1029/2004GL019624, 2004.

Fritts, D. C. and Alexander, M. J.: Gravity wave dynamics and effects in the middle atmosphere, Rev. Geophys., 41(1), 1003, doi:10.1029/2001RG000106, 2003.

Fritts, D. C. and Vincent, R. A.: Mesospheric momentum flux studies at Adelaide, Australia: observations and a gravity wave-tidal interaction model, J. Atmos. Sci., 44, 605–619, 1987.

Fritts, D. C., Tsuda, T., Sato T., Fukao, S., and Kato, S.: Observational evidence of a saturated gravity wave spectrum in the troposphere and lower stratosphere, J. Atmos. Sci., 45, 1741–1759, 1988.

Holton, J. R.: The role of gravity wave-induced drag and diffusion in the momentum budget of the mesosphere, J. Atmos. Sci., 39, 791–799, 1982.

Holton, J. R.: The influence of gravity wave breaking on the general circulation of the middle atmosphere, J. Atmos. Sci., 40, 2497–2507, 1983.

Innis, J. L., Klekociuk, A. R., and Vincent, R. A.: Interstation correlation of high-latitude lower-stratosphere gravity wave activity: Evidence for planetary wave modulation of gravity wave over Antarctica, J. Geophys. Res., 109, D17106, doi:10.1029/2004JD004961, 2004.

Lindzen, R. S.: Turbulence and stress owing to gravity wave and tidal breakdown, J. Geophys. Res., 86, 9707–9714, 1981.

Manzini, E. and McFarlane, N.: The effect of varying the source spectrum of a gravity wave parameterization in a middle atmosphere general circulation model, J. Geophys. Res., 103, 31 523–31 539, 1998.

Manson, A. H., Meek, C. E., Luo, Y., Hocking, W. K., MacDougall, J., Riggin, D., Fritts, D. C., and Vincent, R. A.: Modulation of gravity waves by planetary waves (2 and 16 d): observations with the North American-Pacific MLT-MFR radar network, J. Atmos. Sol-Terr. Phys., 65, 85–104, 2003.

Nastrom, G. D., VanZandt, T. E., and Warnock, J. M.: Vertical wavenumber spectra of wind and temperature from high resolution balloon soundings in the lower atmosphere over Illinois, J. Geophys. Res., 102, 6685–6702, 1997.

Pfenninger, M. A., Liu, A. Z., Papen, G. C., and Gardner, C. S.: Gravity wave characteristics in the lower atmosphere at South Pole, J. Geophys. Res., 104, 5963–5984, 1999.

Ray, E. A., Alexander, M. J., and Holton, J. R.: An analysis of structure and forcing of the equatorial semiannual oscillation in zonal wind, J. Geophys. Res., 103(D2), 1759–1774, 1998.

Scargle, J. D.: Studies in astronomical time series analysis II, statistical aspects of spectral analysis of unevenly spaced data, Astrophys. J., 263, 835–853, 1982.

Seidel, D. J., Free, M., and Wang, J.: Diurnal cycle of upper-air temperature estimated from radiosondes, J. Geophys. Res., 110, D09102, doi:10.1092/2004JD005526, 2005.

Senft, D. C., Hostetler, C. A., and Gardner, C. S.: Characteristics of gravity wave activity and spectra in the upper stratosphere and upper mesosphere at Arecibo during early April 1989, J. Atmos. Terr. Phys., 55, 425–439, 1993.

Shimizu, A. and Tsuda, T.: Characteristics of Kelvin waves and gravity waves observed with radiosondes over Indonesia, J. Geophys. Res., 102, 26 159–26 171, 1997.

Smith, S. A., Fritts, D. C., and VanZandt, T. E.: Evidence for a saturated spectrum of atmospheric gravity waves, J. Atmos. Sci., 44, 1404–1410, 1987.

Tsuda, T., Inoue, T., Fritts, D. C., VanZandt, T. E., Kato, S., Sato, T., and Fukao, S.: MST radar observations of a saturated gravity wave spectrum, J. Atmos. Sci., 46, 2440–2447, 1989.

Tsuda, T., Kato, S., Yokoi, T., Inoue, T., and Yamamoto, M.: Gravity waves in the mesosphere observed with the middle and upper atmosphere radar, Radio Sci., 25, 1005–1018, 1990.

Tsuda, T., VanZandt, T. E., Mizumoto, M., Kato, S., and Fukao, S.: Spectral analysis of temperature and Brunt-Väisälä freuquency frequency fluctuations observed by radiosondes, J. Geophys. Res., 96, 17 265–17 278, 1991.

Tsuda, T., Murayama, Y., Wiryosumarto, H., Harijono, S. W. B., and Kato, S.: Radiosonde observations of equatorial atmosphere dynamics over Indonesia, 1, Equatorial waves and diurnal tides, J. Geophys. Res., 99, 10 491–10 505, 1994a.

Tsuda, T., Murayama, Y., Wiryosumarto, H., Harijono, S. W. B., and Kato, S.: Radiosonde observations of equatorial atmosphere dynamics over Indonesia, 2, Characteristics of gravity waves, J. Geophys. Res., 99, 10 506–10 516, 1994b.

Vincent, R. A. and Alexander, M. J.: Gravity waves in the tropical lower stratosphere: An observational study of seasonal and inter-annual variability, J. Geophys. Res., 105, 17 971–17 982, 2000.

Vincent, R. A., Allen, S. J., and Eckermann, S. D.: Gravity wave parameters in the lower stratosphere, in: Gravity Wave Processes: Their Parameterization in Global Climate models, edited by: Hamilton, K., NATO ASI Ser. I, 50, 7–25, 1997.

Wang L., Geller, M. A., and Alexander, M. J.: Spatial and temporal variations of gravity wave parameters. Part I: Intrinsic frequency, wavelength, and vertical propagation direction, J. Atmos. Sci., 62, 125–142, 2005.

Williams, B. P., Fritts, D. C., She, C. Y., and Goldberg, R. A.: Gravity wave propagation through a large semidiurnal tide and instabilities in the mesosphere and lower thermosphere during the winter 2003 MaCWAVE rocket campaign, Ann. Geophys., 24, 1199–1208, 2006,
http://www.ann-geophys.net/24/1199/2006/.

Wilson, R., Hauchecorne, A., and Chanin, M. L.: Gravity wave spectra in the middle atmosphere as observed by Rayleigh lidar, Geophys. Res. Lett., 17, 1585–1588, 1990.

Yoshiki, M. and Sato, K.: A statistical study of gravity waves in the polar regions based on operational radiosonde data, J. Geophys. Res., 105, 17 995–18 011, 2000.

Zhang, S. D. and Yi, F.: A statistical study of gravity waves from radiosonde observations at Wuhan (30° N, 114° E), China, Ann. Geophys., 23, 665–673, 2005,
http://www.ann-geophys.net/23/665/2005/.

Zhang, S. D. and Yi, F.: Latitudinal and seasonal variations of inertial gravity wave activity in the lower atmosphere over central China, J. Geophys. Res., 112, D05109, doi:10.1029/2006JD007487, 2007.

Zhang, S. D., Huang, C. M., and Yi, F.: Radiosonde observations of vertical wavenumber spectra for gravity waves in the lower atmosphere over central China, Ann. Geophys., 24, 3257–3265, 2006,
http://www.ann-geophys.net/24/3257/2006/.

Zink, F. and Vincent, R. A.: Wavelet analysis of stratospheric gravity wave packets over Macquarie Island, 1. Wave parameters, J. Geophys. Res., 106, 10 275–10 288, 2001a.

Zink, F. and Vincent, R. A.: Wavelet analysis of stratospheric gravity wave packets over Macquarie Island, 2. Intermittency and mean-flow accelerations, J. Geophys. Res., 106, 10 289–10 297, 2001b.